



HAL
open science

.Single-Ion Magnetic Behaviour in an Iron(III) Porphyrin Complex: A Dichotomy Between High Spin and 5/2-3/2 Spin Admixture

Marta Viciano-Chumillas, Geneviève Blondin, Martin Clémancey, Jurek Krzystek, Mykhaylo Ozerov, Donatella Armentano, Alexander Schnegg, Thomas Lohmiller, Joshua Telser, Francesc Lloret, et al.

► To cite this version:

Marta Viciano-Chumillas, Geneviève Blondin, Martin Clémancey, Jurek Krzystek, Mykhaylo Ozerov, et al.. .Single-Ion Magnetic Behaviour in an Iron(III) Porphyrin Complex: A Dichotomy Between High Spin and 5/2-3/2 Spin Admixture. *Chemistry - A European Journal*, 2020, 26 (62), pp.14242-14251. 10.1002/chem.202003052 . hal-02966985

HAL Id: hal-02966985

<https://hal.science/hal-02966985v1>

Submitted on 21 Nov 2022

HAL is a multi-disciplinary open access archive for the deposit and dissemination of scientific research documents, whether they are published or not. The documents may come from teaching and research institutions in France or abroad, or from public or private research centers.

L'archive ouverte pluridisciplinaire **HAL**, est destinée au dépôt et à la diffusion de documents scientifiques de niveau recherche, publiés ou non, émanant des établissements d'enseignement et de recherche français ou étrangers, des laboratoires publics ou privés.

Single-Ion Magnetic Behaviour in an Iron(III) Porphyrin Complex: A Dichotomy Between High-Spin and 5/2–3/2 Spin Admixture

Marta Viciano-Chumillas,^[a] Geneviève Blondin,^{[b]*} Martin Clémancey,^[b] J. Krzystek,^{[c]*} Mykhaylo Ozerov,^[c] Donatella Armentano,^[d] Alexander Schnegg,^[e] Thomas Lohmiller,^[f] Joshua Telser,^[g] Francesc Lloret,^[a] and Joan Cano^{[a]*}

Abstract: We report a mononuclear iron(III) porphyrin compound exhibiting unexpectedly slow magnetic relaxation which is a characteristic of single-ion magnet behaviour. This behaviour originates from the close proximity ($\approx 550 \text{ cm}^{-1}$) of the intermediate-spin $S = 3/2$ excited states to the high-spin $S = 5/2$ ground state. More quantitatively, although the ground state is mostly $S = 5/2$, a spin-admixture model evidences a sizable contribution ($\approx 15\%$) of $S = 3/2$ to the ground state, which as a consequence experiences large and positive axial anisotropy ($D = +19.2 \text{ cm}^{-1}$). Frequency-domain EPR allowed us to directly access the $m_S = |\pm 1/2\rangle \rightarrow |\pm 3/2\rangle$ transitions, thus unambiguously measuring the very large zero-field splitting (ZFS) in this $3d^5$ system. Other experimental results including magnetization, Mössbauer, and field-domain EPR (HFEP) studies are consistent with this model, which is also supported by theoretical calculations.

Introduction

The design of molecules that show nanomagnet behaviour, collectively called single-molecule magnets (SMMs), has been a challenge in the last decades.^[1] The main rationale for this trend has been their (still hypothetical) applications as miniaturized memory units or quantum computing qubits.^[2–7] Initial attention focussed on polynuclear complexes such as the archetypal Mn_{12} or Fe_8 clusters.^[1] The single-magnet properties of such systems are reasonably well understood and depend on the energy barrier between the ground $| -m_S \rangle$ and $| +m_S \rangle$ states, which in turn requires a negative axial zero-field splitting (ZFS, $D < 0$). More recently, the effort has increasingly concentrated on coordination complexes with a single paramagnetic centre, commonly known as mononuclear SMMs or single-ion magnets (SIMs).^[8–11] The reason is to achieve a better control of the magnetic anisotropy compared to polynuclear complexes. In polynuclear systems the effective ZFS parameter of a cluster is a function of the ZFS of all the constituents, which differ in orientation and often in magnitude as well, making the ZFS hard to predict and control. Even magnetic couplings between the paramagnetic centres can make some contribution to the magnetic anisotropy. On the contrary, in SIMs the magnetic anisotropy results from the ligand (or in the case of f-ions, crystal) field of a single metal ion and its spin-orbit coupling (SOC).

A general prerequisite of an SMM is slow relaxation of the magnetization. However, in SIMs, unlike in clusters, the requirement of an energy barrier imposed by a $D < 0$ has been recently questioned by the observation of slow relaxation in cobalt(II) complexes with $D > 0$,^[12–18] or even in systems of $S = 1/2$ spin ground state based on Cu(II) or Ce(III) ions.^[19–22] Moreover, the need for an external magnetic field to observe a slow relaxation of the magnetization in most SIMs (field-induced SIMs) raises additional questions.^[8–11] Indeed, magnetic relaxation is determined by different mechanisms, which are difficult to discriminate and quantify. Therefore, fundamental studies of SIMs are still needed to investigate and understand the processes and mechanisms responsible for the slow relaxation of their magnetization. The most promising hypothesis to date, and recently proposed, it suggests that the spin-lattice relaxation occurs through a spin-phonon coupling.^[7,23–27]

The most productive candidate for 3d metal complexes exhibiting SIM behaviour has so far been the $3d^7$ cobalt(II) ion ($S = 3/2$; $t_{2g}^5 e_g^2$), as recently reviewed.^[8–11] Conversely, the high-spin $3d^5$ iron(III) ion ($S = 5/2$; $t_{2g}^3 e_g^2$) in an octahedral ligand field is an unlikely candidate because it is generally electronically isotropic ($D \approx 0$).^[28] This is due to the negligible orbital contribution in the free-ion ground state, so that SOC acts only in second-order. However, intermediate spin ($S = 3/2$) iron(III) complexes have proven in a few recent examples to be anisotropic, presenting a magnetization reversal barrier.^[29–31]

- [a] Dr. M. Viciano-Chumillas, Prof. F. Lloret, and Dr. J. Cano*
Institut de Ciència Molecular (ICMol)
Universitat de València
46980 Paterna, Spain.
E-mail: joan.cano@uv.es
- [b] Dr. G. Blondin, Dr. M. Clémancey
Univ. Grenoble Alpes, CNRS, CEA, IRIG, CBM
CEA-Grenoble, F-38000 Grenoble, France.
- [c] Dr. J. Krzystek, Dr. M. Ozerov
National High Magnetic Field Laboratory
Florida State University
Tallahassee, FL 32310, USA
- [d] Dr. D. Armentano
Dipartimento di Chimica e Tecnologie Chimiche (CTC),
Università della Calabria
87030 Rende, Cosenza, Italy
- [e] Dr. A. Schnegg
EPR Research Group
MPI for Chemical Energy Conversion
Stiftstraße 34-36, 45470 Mülheim Ruhr, Germany
- [f] Dr. T. Lohmiller
EPR4Energy Joint Lab
Department Spins in Energy Conversion and Quantum Information
Science
Helmholtz-Zentrum Berlin für Materialien und Energie
Kekuléstr. 5, D-12489 Berlin, Germany
- [g] Prof. Dr. J. Telser
Department of Biological, Physical and Health Sciences
Roosevelt University
430 S. Michigan Avenue, Chicago, IL 60605, USA
Supporting information for this article is given via a link at the end of the document

Porphyrins constitute good ligands for the design of SIMs.^[32,33] In particular, iron(III) porphyrins are known to have ground spin states dependent on the ligand strength, especially that of axial ligands.^[34–36] While six-coordinate complexes with strong field axial ligands such as imidazole and cyanide present a low-spin state ($S = 1/2$), five-coordinate complexes with an anionic ligand such as a halide exhibit a high-spin state ($S = 5/2$). In rare cases, an intermediate spin ($S = 3/2$) occurs with weak anionic ligands. Maltempo showed, however, that yet another case is possible, namely a quantum spin-admixed ground state.^[37] In such a case the wavefunction of the ground state is composed of both the $S = 3/2$ and $S = 5/2$ spin states, rendering them no longer good quantum numbers.^[38]

Herein we present a mononuclear iron(III) compound, $[\text{Fe}(\text{TPP})(\text{H}_2\text{O})_2]\text{ClO}_4$ (**1**), where TPPH₂ is 5,10,15,20-tetraphenyl-21*H*,23*H*-porphine (*meso*-tetraphenylporphyrin). Scheidt and co-workers previously reported compounds with the same iron(III)-porphyrin unit exhibiting structural parameters similar to those found in **1**,^[39,40] but no detailed investigation of their magnetic properties was reported. Compound **1** is a mononuclear iron(III) complex behaving very much as a high-spin system ($S = 5/2$) with a large positive axial magnetic anisotropy. We demonstrate that **1** is the first high-spin ferric complex with $D > 0$ exhibiting slow magnetic relaxation, with a blocking of the magnetization that is most likely related to spin-lattice relaxation. Detailed high-frequency and -field electron paramagnetic resonance (HF-EPR) and Mössbauer spectroscopic measurements hint at the magnitude and prove the sign of the ZFS. Frequency-domain magnetic resonance techniques, alternatively called frequency-domain Fourier-transform THz-EPR (FD-FT THz-EPR) or far-infrared magnetic spectroscopy (FIRMS), allow us to probe the excitation from the $m_S = |\pm 1/2\rangle$ ground to the $m_S = |\pm 3/2\rangle$ first excited Kramers doublet, which directly determines the ZFS in **1**. The large magnitude of ZFS is supported and explained by quantum-chemical calculations.

Results

Synthesis and crystal structure

Recrystallization from xylene solution under aerobic conditions of the solid obtained by reaction of $[\text{Fe}(\text{TPP})\text{Cl}]$ and AgClO_4 in hot THF yielded **1** (details in Supporting Information (SI)). Thermogravimetric analysis (TGA) of **1** shows a mass loss of 4% above 150°C, which is in agreement with the loss of two water molecules (Figure S1), proving its stability at room temperature. Thus, the bis-aqua axial coordination to the iron(III) ion seen in the room temperature crystal structure (Figure 1) is intact at the lower temperatures used for all physical / spectroscopic measurements. Crystallographic (Table S1) and structural data (Table S2) can be found in the SI. The iron(III) ion is in an elongated octahedral coordination geometry, exactly in the equatorial plane formed by the porphyrin nitrogen atoms, as expected for a metalloporphyrin with two identical axial ligands. The Fe–N distances are 2.024(3) and 2.038(4) Å, while the Fe–O distance (axial) is 2.130(3) Å. The *cis* N–Fe–N angles are 89.7(1)° and 90.3(1)°, whereas the

O–Fe–O and *trans* N–Fe–N angles are linear. The coordination geometry of the iron(III) ion is thus not far from an ideal octahedron even if there are modest tetragonal and rhombic distortions. These data are consistent with other reported high-spin $S = 5/2$ iron(III) porphyrin complexes.^[34,39,40] Hydrogen bonding is present between the coordinated water molecules and the perchlorate anion, giving rise to chains (Figure S2 and Table S3) with a Fe...Fe distance of 10.33 Å. The shortest Fe...Fe intermolecular distance is 8.03 Å between iron(III) ions of adjacent chains.

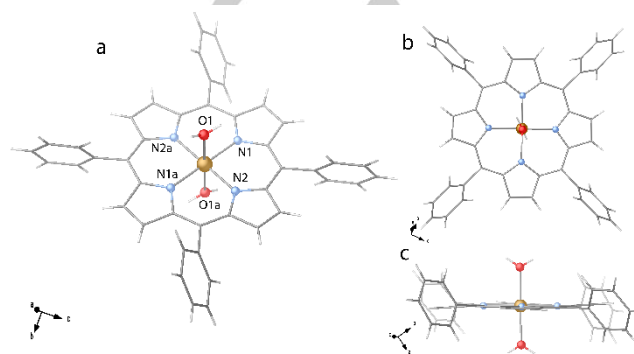


Figure 1. Perspective drawing (a) and top (b) and side (c) views of the cationic mononuclear iron(III) unit of **1**. Colour code: brown, iron; blue, nitrogen; red, oxygen; grey, carbon; white, hydrogen.

Static magnetic properties

The direct current (dc) magnetic properties of **1** were measured as $\chi_M T$ vs T and M vs H/T , as shown in Figure 2. The $\chi_M T$ value of **1** at room temperature ($3.56 \text{ cm}^3 \text{ K mol}^{-1}$) is lower than previously reported^[39] and than the spin-only value for $S = 5/2$ ($4.37 \text{ cm}^3 \text{ K mol}^{-1}$), but significantly higher than the value for $S = 3/2$ ($1.87 \text{ cm}^3 \text{ K mol}^{-1}$). This $\chi_M T$ value slightly increases when cooling to reach $3.68 \text{ cm}^3 \text{ K mol}^{-1}$ at 140 K and then decreases to $2.30 \text{ cm}^3 \text{ K mol}^{-1}$ at 5 K. This behaviour is characteristic of iron(III) complexes showing a $5/2$ – $3/2$ spin-admixed ground state and is due to the presence of higher-lying quartet states close in energy to the sextet ground state. This proximity in energy, modelled through the appropriate choice of crystal field strengths,^[37,38,41] promotes a notable interaction between these states, leading to a ground state that is best described as a mixture of a sextet and one or more quartet electronic configurations. Additionally, the depopulation of these nearby quartet states in favour of the sextet ground state when cooling causes a slight and gradual increase of $\chi_M T$ in the high-temperature region. The magnetization value at 5 T and 2 K is $2.72 \text{ N}\beta$ (Figure 2 inset). This value is below the saturation limit of $5 \text{ N}\beta$ for one $S = 5/2$ ion with $g = 2$. The isothermal magnetization curves in the 2 – 10 K temperature range do not superimpose at high H/T values, suggesting a significant ZFS since the iron(III) ions are magnetically well isolated (Fe...Fe distance $> 8 \text{ Å}$).

The physical principles underlying the spin-admixed and ZFS models are the same, and only the amplitude of the interaction between the sextet ground and nearest quartet excited states determines the point at which one model is more suitable than the

other. Owing to the small change in $\chi_M T$ at high temperature (300 – 40 K) pointing to a modest extent of spin-admixture, the lowest-lying Kramers doublets can be described by a ZFS model for $S = 5/2$. Although analysis of the $\chi_M T$ vs. T plot at higher temperatures using the ZFS model is limited, adding a temperature-independent paramagnetism (TIP) that accounts for a depopulation of the first quartet excited state with decreasing temperature is a useful alternative to the spin-admixed model.^[42–44] Such depopulation on cooling can lead to an increase of the $\chi_M T$ product and a negative value of the TIP.

The experimental magnetic susceptibility and magnetization data of **1** were fitted with the VPMAG program^[45] using a standard spin-Hamiltonian for $S = 5/2$ [$\hat{H}_{\text{Spin}} = \hat{H}_{\text{Zeeman}} + \hat{H}_{\text{ZFS}} = \mu_B B_0 g S + D(\hat{S}_z^2 - \frac{1}{3}S(S+1)) + E(\hat{S}_x^2 - \hat{S}_y^2)$], being D and E the axial and rhombic ZFS parameters. The obtained best-fit parameters are: $D = +17.9 \text{ cm}^{-1}$, $E/D = 0.002$, $g_{\perp} = 1.84$, $g_{\parallel} = 2.03$, and $\text{TIP} \times 10^6 = -1091.3 \text{ cm}^3 \text{ mol}^{-1}$ with $F = 1.8 \times 10^{-5}$ (F is the agreement factor defined as $\Sigma[P_{\text{exp}} - P_{\text{calcd}}]^2 / \Sigma[P_{\text{exp}}]^2$, with P being the physical property under study).

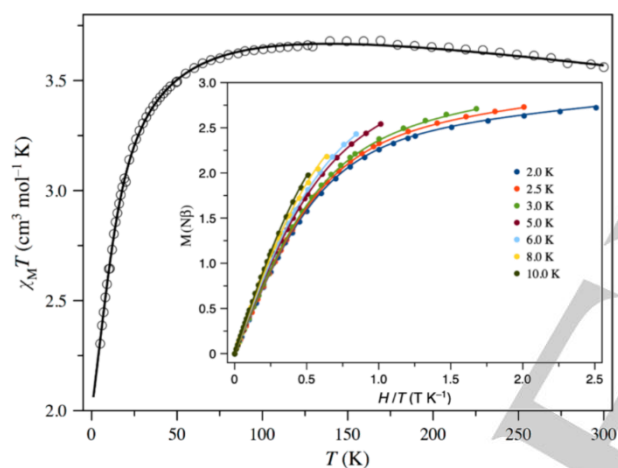


Figure 2. Plots of $\chi_M T$ vs. T in the range 2 – 300 K at 0.025 T ($T < 20$ K) and 0.5 T ($T \geq 20$ K) applied field and M vs. H/T (inset) for **1** in the 2 – 10 K temperature range. The solid lines are the best-fit curves (see text).

Magnetic resonance spectroscopy

Frequency-domain Fourier-transform (FD-FT) THz-EPR, or far-infrared magnetic spectroscopy (FIRMS), allows a direct, highly accurate and precise measurement of large ZFS.^[46,47] Low-temperature (4.6 K) FD-FT THz-EPR spectra of **1** recorded up to 4.5 T at the BESSY II facility (Berlin) are shown in Figure 3. They are depicted as magnetic-field division spectra (MDS), in which the measured spectral intensities at the indicated fields are divided by each other in order to remove all signals from non-magnetic transitions, invariant to the field, from the spectra. The experiment was repeated independently at NHMFL (Tallahassee), with the resulting spectra shown in Figure S3, using a different method to suppress the non-magnetic transitions (see Experimental Section). In both experiments, we could observe the intra-Kramers $m_s = |-1/2\rangle \rightarrow |+1/2\rangle$ transition that is shifted by the magnetic field into the observation window of the BESSY II

synchrotron-based experiment, as observed in the 4.5 T / 4 T spectrum. Similarly, application of magnetic fields above 6 T shifts this transition into the observation window of the FIRMS experiment at NHMFL. More importantly, we were able to observe in both experiments the inter-Kramers $m_s = |\pm 1/2\rangle \rightarrow |\pm 3/2\rangle$ transitions. In the 1 T / 0 T FD-FT THz-EPR spectrum, the ZFS energy can be directly determined from that transition as $\Delta = 2\sqrt{D^2 + 3E^2} = 38.5 \text{ cm}^{-1}$ (Figure 3). The FIRMS experiment (Figure S4) yielded $\Delta = 38.3 \text{ cm}^{-1}$. A consensus value for Δ between the two independent experiments can thus be safely assumed as $38.4(1) \text{ cm}^{-1}$. Since the ZFS tensor of complex **1** is almost exactly axial (see below), this yields the axial ZFS parameter $D = \Delta/2 = +19.2 \text{ cm}^{-1}$.

We have also performed a least-squares fitting of simulations to the field-dependent MDS which yielded further spin Hamiltonian parameters; $g_{\perp} = 1.87$, $g_{\parallel} = 2.00$ (fixed), $E = 0.28 \text{ cm}^{-1}$ ($E/D \approx 0.015$). A D strain $\Delta D = 1.6 \text{ cm}^{-1}$ ($\Delta D/D = 7.8\%$) was found to be necessary to be included to account for the observed line widths. The field dependence of the sublevel energies of the $S = 5/2$ spin manifold is shown in Figure S5.

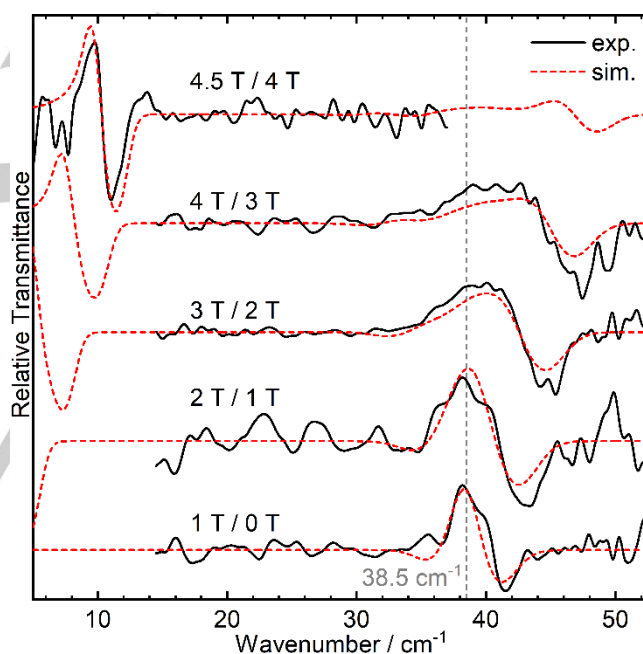


Figure 3. Experimental FD-FT THz-EPR MDS of **1** measured at 4.6 K (black solid line) and simulations thereof (red dashed line). Spectra depicted above 14 cm^{-1} were acquired using the Hg arc lamp of the FTIR spectrometer, the spectrum at the top depicted in the range $5 - 37 \text{ cm}^{-1}$ using synchrotron radiation (BESSY II, low- α mode). In the relative transmittance MDS obtained by division of a raw spectrum at $B_0 + 1 \text{ T}$ by one measured at B_0 , respectively at 4.5 T by one at 4 T, maxima correspond to stronger absorption at lower B_0 , minima to increased absorption at higher B_0 .

Field-domain experiments were conducted in the form of HFEP in a 100 – 650 GHz frequency range. A typical low temperature spectrum is shown in Figure S6 and is symptomatic of $S = 5/2$ and positive D much larger than the sub-THz wave energy quantum, consisting exclusively of turning points of the intra-Kramers $m_s = |-1/2\rangle \rightarrow |+1/2\rangle$ transition. In such a case, typically no information

on the ZFS parameter D can be obtained; however, we used the D value known from frequency-domain experiments (19.2 cm^{-1}) as a constant, and subjected the other $S = 5/2$ spin Hamiltonian parameters to a fit using the tunable-frequency methodology,^[48] as depicted in Figure S7. In this way, we obtained the values: $E = 0.28 \text{ cm}^{-1}$, $g_{\perp} = 1.87$, $g_{\parallel} = 2.00$, which agree very well with the frequency-domain results. Note that E in HFEPR was obtained from the visible splitting of the perpendicular turning point of the intra-Kramers transition (Figure S6), which is not resolved in the frequency-domain experiment (Figure 3). Although in principle that splitting can also originate from in-plane g anisotropy ($g_x \neq g_y$), it is far more sensitive to the rhombicity of the ZFS tensor than to that of the g tensor. We can thus conclude that $E/D \approx 0.015$. These results agree with the fits of the magnetometric and Mössbauer data (see below and Table 1). Specifically, the low g_{\perp} value is confirmed and responsible for the low $\chi_M T$ value at room temperature.

Mössbauer spectroscopy

Figure 4 presents the Mössbauer spectrum recorded on a powder sample of **1** at 5 K with a 7 T external magnetic field applied perpendicular to the γ -radiation (hatched bars). Additional spectra are presented in Figure S9. Previously published measurements were performed at 78 and 298 K in zero field, allowing only the determination of the isomer shift and quadrupole splitting.^[39] All the Mössbauer spectra of **1** are also very similar to those reported for the picket-fence porphyrin complex, [(TPpivP)Fe^{III}(OSO₂CF₃)(OH₂)].^[49] Given the large D -value obtained by magnetometry and magnetic resonance, we considered multiple approaches to spectral analysis. In a first approach, an axial symmetry was assumed. Assuming **1** is a pure $S = 5/2$ system, simultaneous fitting of the six spectra reported in Figures 4 and S9, leads to the following electronic and nuclear parameters: $D = +18 \pm 3 \text{ cm}^{-1}$, $g_{\perp} = 1.88 \pm 0.10$, $g_{\parallel} = 2.0$ (fixed), $A_{\perp}/(g_N \mu_h) = -17.7 \pm 0.2 \text{ T}$, $A_{\parallel}/(g_N \mu_h) = -29 \pm 3 \text{ T}$, $\Delta E_Q = 2.0 \pm 0.1 \text{ mm s}^{-1}$ for $T < 100 \text{ K}$, $\Delta E_Q = 2.15 \pm 0.20 \text{ mm s}^{-1}$ for $T > 100 \text{ K}$, $\delta = 0.43 \pm 0.03 \text{ mm s}^{-1}$ for $T < 100 \text{ K}$ and $\delta = 0.41 \pm 0.10 \text{ mm s}^{-1}$ for $T > 100 \text{ K}$ (see solid lines in Figures 4 and S9). In a second step, fits were performed assuming rhombic ZFS. The quality of the simulations was not significantly improved and the E/D ratio was < 0.02 , validating the initially assumed axial symmetry. The D and g_{\perp} parameters were also found in excellent agreement with the values deduced from the magnetic data and from the frequency- and field-domain EPR measurements.

Compound **1** was alternatively analysed as a spin-admixed ($S = 5/2-3/2$) system as had been reported for [(TPpivP)Fe^{III}(OSO₂CF₃)(OH₂)].^[49] Equally satisfying simulations were obtained for the six Mössbauer spectra, as shown in Figure S10. Within this model, developed in the 1970's by Maltempo,^[37,50] the critical electronic parameters are the single-electron SOC constant (ξ) and, in a D_{2h} symmetry, the energy gap between the ground 6A_g and the excited ${}^4B_{1g}$ states ($\Delta_{3/2-5/2}$), taken as positive here for the $S = 5/2$ ground state. The obtained values are $\Delta_{3/2-5/2} = 550 \pm 50 \text{ cm}^{-1}$ and $\xi = 230 \pm 20 \text{ cm}^{-1}$, indicating that the ground spin state has a dominant $S = 5/2$ character ($86 \pm 3\%$), but also a significant contribution ($14 \pm 3\%$) of the first $S = 3/2$ excited spin state. The relationship between spin-admixed and

ZFS models is expressed through equations S3 and S4, and in agreement with magnetometry and FD-FT THz-EPR and HFEPR spectroscopies, this result leads to values of $D = +20 \pm 3 \text{ cm}^{-1}$ and $g_{\perp} = 1.91 \pm 0.02$.

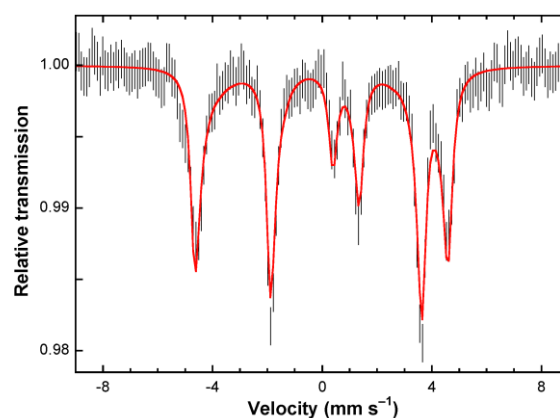


Figure 4. Experimental Mössbauer spectrum of **1** recorded at 5 K with a 7 T external magnetic field applied perpendicular to the γ -beam (hatched bars). The solid red line is a simulation obtained with parameters given in the text for a pure axial $S = 5/2$ spin system.

Computational studies

Ligand-field theory (LFT) can first be used to provide a simple picture as to the origin of the spin Hamiltonian parameters in high-spin d^5 complexes. The major contributions of quartet excited states to the ZFS parameter and the g -values are described by the following equations for D_{2h} symmetry:^[51]

$$D = \frac{\xi^2}{10} \left[\frac{2}{E({}^4B_{1g})} - \left(\frac{1}{E({}^4B_{2g})} + \frac{1}{E({}^4B_{3g})} \right) \right] \quad (1)$$

$$E = \frac{\xi^2}{10} \left[\frac{1}{E({}^4B_{2g})} - \frac{1}{E({}^4B_{3g})} \right] \quad (2)$$

$$g_{\perp} = g_e - \frac{\xi}{5} \frac{2}{E({}^4B_{1g})} \quad (3)$$

$$g_{\parallel} = g_e + \frac{\xi}{5} \left(\frac{1}{E({}^4B_{2g})} + \frac{1}{E({}^4B_{3g})} \right) \quad (4)$$

where g_e is the free-electron g -value (~ 2.00) and the relative energies of various quartet excited states are given by $E({}^4B_{1g})$, etc. Similar equations have been used with the Maltempo model for the Mössbauer spectroscopy simulations (see SI). The ${}^4B_{1g}$ state contributes oppositely to D versus the ${}^4B_{2g}$ and ${}^4B_{3g}$ states, but since the first of these is much lower in energy in a tetragonal system, the sign of D is positive (see Figure S11). This contribution of the ${}^4B_{1g}$ state also leads to a deviation of g_{\perp} from g_e to a lower value (see equation 3), while g_{\parallel} deviates above g_e (see equation 4) due to the interaction with the other two quartet states. A reduction of the molecular symmetry from D_{4h} to D_{2h} infers an energy gap between the ${}^4B_{2g}$ and ${}^4B_{3g}$ states leading to rhombicity of the ZFS tensor ($E \neq 0$, see equation 2). This splitting is small since the porphyrin ligand enforces nearly four-fold symmetry (see Table S4).

FULL PAPER

DFT calculations were performed to reproduce the experimental results and analyse their origin. DFT calculations based on the broken-symmetry approach were also employed on models with two neighbouring iron-porphyrin units to confirm the absence of intermolecular magnetic interactions. Using the crystallographic geometry, the calculated ZFS parameters for a spin sextet ($D = +23.8 \text{ cm}^{-1}$, $E/D = 0.27$) support the large and positive D value but not the small E/D ratio, which is usually more difficult to evaluate by theoretical methods. However, when the calculations are done on the optimized geometry, the resulting E/D ratio is lower than 0.005 (see Table S5). The spin-spin coupling (SSC) contribution to ZFS is always negligible (around 0.02%), and the SOC contribution is almost entirely from the quartet excited states, as equation 1 and the spin-admixed model used to analyse the Mössbauer data suggest. An evaluation of the relative energies of the excited states by DFT methods is difficult, particularly when the ground and excited states exhibit different spin multiplicity, resulting in over-stabilized excited states. Only sophisticated techniques such as the constrained-DFT method can help to solve this problem.^[52–55] However, changing the occupation of the frozen single-occupied molecular orbitals (SOMOs) composed mostly of d orbitals of the iron(III) ion and avoiding any relaxation of the wavefunction can provide a better approach for the energies of the quartet excited states, although slightly overestimated. This approach, not detailed here, suggests that the first quartet excited state should be placed at only 1000 cm^{-1} (E_1). Other theoretical results using *ab initio* post-Hartree-Fock methods and the problem to cover the covalence of the metal-ligand bond fully through dynamical correlation are further discussed in the SI (Figures S12 and S13).

Table 1. Spin Hamiltonian parameters for **1** obtained from different techniques.

Technique	g_{\perp}	g_{\parallel}	D^a	E/D
Magnetometry	1.84	2.03	+17.9	0.002
FD-FT THz-EPR	1.87	2.00 ^b	+19.25	0.015
FIRMS	1.87	2.00 ^b	+19.15	–
HFEPR	1.88	2.00	+19.2 ^b	0.015
Mössbauer ($S = 5/2$ model analysis)	1.88 ± 0.10	2.0 ^b	+18 ± 3	<0.02
Mössbauer ($S = 5/2$ – $3/2$ spin admixed model analysis)	1.91 ± 0.02^c	2.0 ^b	+20 ± 3 ^c	–

^a in cm^{-1} , ^b fixed value, ^c calculated according to equations S3 and S4.

Dynamic magnetic properties

Alternating current (ac) magnetic susceptibility studies of **1** were performed to study its relaxation properties. No χ_M'' signals were observed down to 1.9 K in absence of a dc-magnetic field even at the highest frequency used (10 kHz). However, a frequency-dependent component appears both in χ_M' and χ_M'' below ca. 5 K

in the presence of an applied field (Figures 5, S14–S17). The presence of a dc-magnetic field usually hampers relaxation through a quantum tunnelling mechanism (QTM) and nonzero χ_M'' signals are observed. The QTM is typically observed for SMM systems possessing large negative D values and high energy barriers.^[1] However, no barrier occurs for systems exhibiting easy-plane slow relaxation magnetization ($D > 0$), a common feature in 3d SIMs.^[8–11] In these cases, an intra-Kramers transition within the magnetic ground Kramers doublet rather than QTM should be invoked to describe the SIM behaviour.

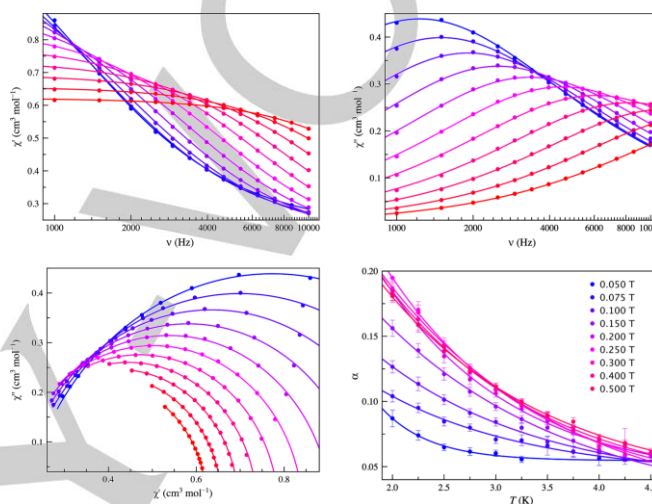


Figure 5. Frequency dependence of χ_M' (top left) and χ_M'' (top right), and Cole-Cole plots (bottom left) of **1** under a dc-applied static field of 0.15 T with ± 0.5 mT oscillating field in the temperature range of 2 – 4.5 K (from blue to red). Thermal dependence of α (bottom right) under dc-applied static fields from 0.05 to 0.5 T. Standard deviations appear as vertical error bars.

The experimental data were analysed through a Debye model described by the parameters χ_S , χ_T , τ , and α , which are the static and infinite frequency magnetic susceptibilities, the relaxation time, and the exponential factor respectively, the last one describing the spectral breadth. The simultaneous fit of χ_M' and χ_M'' vs ν is the best approach,^[56] which nicely reproduces $\chi_M'-\nu$, $\chi_M''-\nu$, and the Cole-Cole plots with a unique set of values (Figures 5, S14–S17). Moreover, the standard errors for the parameters are usually smaller than those through the analysis of the Cole-Cole plots. Nevertheless, the correlation matrices point out that the fit parameters are not independent. Also, the values of α decrease in the temperature range $2.0 \text{ K} \leq T \leq 4.5 \text{ K}$, but they continuously increase for $T > 4.5 \text{ K}$ (Figure 5). Either the high correlation among the parameters or the presence of a second relaxation process could account for this last anomaly. In fact, despite the low values of χ_M'' , an additional weak signal in the $\chi_M''-\nu$ plots is discerned above 7 K (Figure S18). These issues combined limited our analysis to the data at $T \leq 4.5 \text{ K}$.

The obtained results are illustrated by the Figures 5 and 6, where $\alpha < 0.2$ at any temperature and under any explored dc magnetic field (0.075 – 0.5 T). This feature supports a single relaxation process and rejects any spin-glass behaviour. On the other hand,

the temperature dependent relaxation times, $\tau = 1/2\pi\nu$, as Arrhenius plots, begin to superimpose as the applied dc magnetic field increases up to 0.3 T. At higher fields, other relaxation mechanisms emerge. Thus, these curves were fitted by using any of the following combinations of relaxation mechanisms: Raman plus direct [$1/\tau = CT^n + AT$], Orbach and direct [$1/\tau = (1/\tau_0)\exp(-E_a/k_B T) + AT$], and two Orbach processes [$1/\tau = (1/\tau_{01})\exp(-E_{a1}/k_B T) + (1/\tau_{02})\exp(-E_{a2}/k_B T)$].

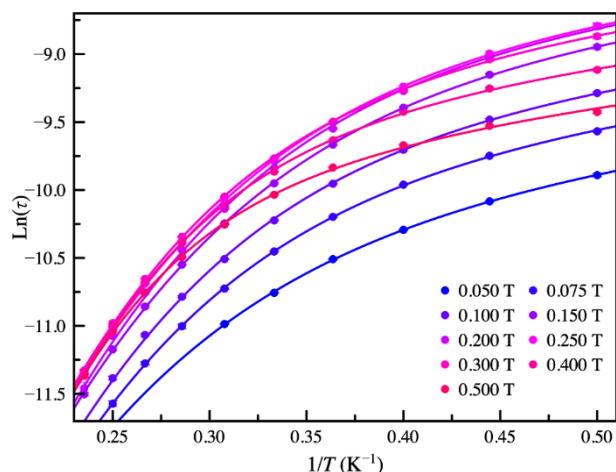


Figure 6. Arrhenius plots for **1** under applied static fields from 0.05 to 0.5 T. The solid lines are the best fit-curves using a model that combines Raman and direct processes. Standard deviations appear as vertical error bars.

Due to the positive value of D , the Orbach process is not related to an energy barrier arising from the ZFS, but to the need for reaching a most likely vibrational excited state to allow a fast relaxation. Concerning the Raman plus direct combination, although the values of n (5.2 – 7.2) are roughly in the physically expected range (6 – 8), they depend on the magnetic field. Still, this unusual dependence on the magnetic field also occurs for the C parameter (Raman, Figure 7top) and the coefficient for the direct relaxation does not follow the expected dependence ($A \propto H^2$) (Figure 7bottom).^[57] The latter observation is also reproduced in the case of Orbach plus direct mechanisms (Figure S19). Finally, the values of the energy barrier (E_a) for the Orbach-direct combination cover the range 14 – 19 cm^{-1} under most of the applied dc fields, with somewhat smaller values at the lowest magnetic fields following a linear dependence.

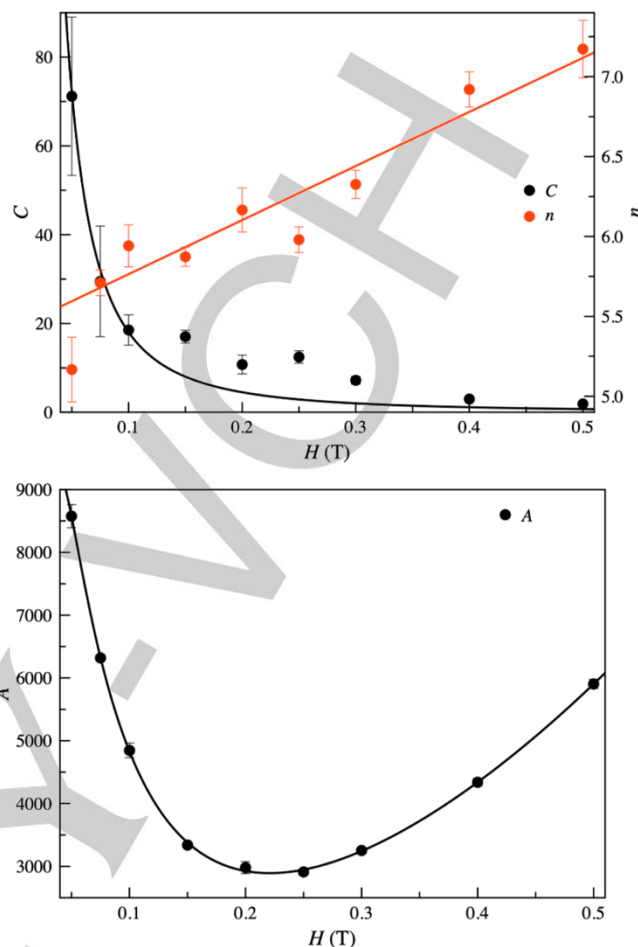


Figure 7. Dependence of the parameters defining a model that combines Raman (top; parameters C and n ; see text) and direct (bottom; parameter A ; see text) relaxation mechanisms on the applied dc magnetic field for **1**. Standard deviations appear as vertical error bars.

Discussion

Up to now, the few reported iron(III) SIMs have displayed negative values of the anisotropy in the range from -1.2 to -50 cm^{-1} with an $S = 3/2$ ground state.^[29–31] A high-spin $3d^5$ complex should be magnetically isotropic ($D = 0$), but the proximity of the excited quartet ($S = 3/2$) states, which depends on the ligand fields, can significantly affect the ground state, inducing anisotropy. Only recently, SIM behaviour (with $D < 0$), was observed for $S = 5/2$ iron(III) compounds.^[58–60] The ground state in iron(III) porphyrins in particular can be tuned by the ligand field, as observed in such complexes displaying $S = 1/2$, $3/2$, and $5/2$ ground states,^[34–36] including those with $S = 5/2$ and positive and sizable D values.^[61–63] In **1**, the ligand field of the water molecules at axial positions is not strong enough to induce an intermediate $S = 3/2$ ground state,^[64] but is sufficient to bring the quartet excited states close

in energy and thus to induce magnetic anisotropy and SIM behaviour in the presence of an external magnetic field.

The low $\chi_M T$ value at room temperature, its unusual high-temperature behaviour and the Mössbauer spectroscopy study indicate the presence of at least one very close excited quartet state ($545 \pm 50 \text{ cm}^{-1}$). This fact not only explains the large ZFS found in **1**, but it also suggests the occurrence of a slight spin-admixture in such a way that the ground state no longer corresponds to a pure sextet state but a mixture with a quartet state in an 86:14 ratio.

The magnetic relaxation process for systems with m_S states close in energy is typically due to the presence of an energy barrier attributed to an axial $D < 0$ anisotropy, as occurs in manganese(III) compounds.^[32,65,66] However, in systems with large ZFS like octahedral cobalt(II) complexes, the sign of the anisotropy is not decisive to observe slow magnetic relaxation because different mechanisms, e.g. spin-phonon coupling, direct and Raman processes, can be responsible for such behaviour.^[67] Since there is no energy barrier ($D > 0$) in **1**, the lowest molecular vibrational frequencies might instead be the basis for the slow magnetic relaxation.^[7,24,25,27,68–71] At temperatures in which no excited vibrational level is significantly occupied, the magnetization cannot effectively relax and it is blocked. However, a slight increase in temperature populates the first levels of the low-lying vibrational modes in the molecule, or by extension, phonons in the lattice, causing greater dynamics that favour a faster relaxation of the magnetization. Theoretical analysis of low energy vibrational modes was done (see SI, which includes videos of the first three vibrational modes) to understand the magnetic relaxation. These vibrational modes correspond mainly to motions involving the phenyl rings of the porphyrin. The first vibrational mode appears at 12.5 cm^{-1} and the next around 25 cm^{-1} , which is consistent with a non-magnetic transition observed at 21.6 cm^{-1} in FD-FT THz-EPR spectra (Figure S8). The first observed relaxation process thus might be related to relaxation through spin-phonon coupling. It is worth noting that a spin-lattice relaxation phenomenon was proposed to be the preponderant mechanism responsible for the intermediate electronic relaxation process detected by Mössbauer spectroscopy for [(TPpivP)Fe(OSO₂CF₃)(OH₂)].^[49] Owing to the similarity of the nuclear and electronic parameters for both complexes, this experimental evidence supports our conjecture on the role of vibrational modes in **1**.

Conclusions

We report here the first example of a mononuclear high-spin d^5 ($S = 5/2$) iron(III) compound, in the form of the six-coordinate porphyrin complex **1**, that shows both an in-plane magnetic anisotropy and SIM behaviour with applied external magnetic field. Despite the expected isotropic spin ground state, the compound displays a large and positive magnetic anisotropy value (axial ZFS with $D = +19.2 \text{ cm}^{-1}$), which can be attributed to the contribution of quartet excited states (i.e., a spin-admixed character to the ground state). Magnetization, field- and frequency-domain magnetic resonance techniques, and Mössbauer measurements

confirm this result, which is also supported by theoretical calculations. The slow relaxation of the magnetization of **1** may be modulated by low-energy molecular vibrational modes. Future work will explore the role of axial ligands in this class of porphyrinic compounds to clarify their effect on the SIM behaviour and how they can relate to the low-energy molecular vibrational modes.

Experimental Section

Materials: All chemicals were obtained from commercial sources and used as received. [Fe(TPP)Cl] was synthesized as described in the literature.^[72] **Caution!** Perchlorate salts are potentially explosive. They should be used in small quantities and be treated with utmost care at all times.

Synthesis of [Fe(TPP)(H₂O)₂]ClO₄ (1**):** [Fe(TPP)Cl] (203 mg, 0.288 mmol) and AgClO₄ (78 mg, 0.373 mmol) were dissolved in boiling THF and stirred during few minutes under aerobic conditions. After filtration, heptane was added to the solution affording purple crystals that were collected by filtration. Single crystals of **1** were obtained by recrystallization of the solid with xylene solution under aerobic conditions. Yield: 169 mg (73%). IR ($\nu_{\text{max}}/\text{cm}^{-1}$): 3520(s, coordinated H₂O) and 1072(br, ClO₄⁻).

Physical measurements: Infrared spectra (4000–300 cm^{-1}) were recorded on a Nicolet 5700 spectrophotometer as KBr pellets. The thermogravimetric analysis (TGA) was performed on single-crystals of **1** under a dry N₂ atmosphere with a Mettler Toledo TGA/STDA 851e thermobalance in the temperature range 25 to 250 °C.

Static direct current (dc) measurements were carried out on **1** by powdering and restraining the samples in order to prevent any displacement due to the magnetic anisotropy. Variable-temperature (2.0–300 K) dc-magnetic susceptibility under an applied field of 0.025 ($T < 20 \text{ K}$) and 0.5 T ($T \geq 20 \text{ K}$), and variable-field (0–5.0 T) magnetization in the temperature range from 2 to 10 K were recorded with a Quantum Design SQUID magnetometer. Variable-temperature (2.0–10 K) alternating current (ac) magnetic susceptibility measurements under $\pm 0.5 \text{ mT}$ oscillating field at frequencies in the range of 0.1–10 kHz were carried out on crystalline samples under different applied static dc-fields in the range 0.0–0.5 T with a Quantum Design Physical Property Measurement System (PPMS). The magnetic susceptibility data were corrected for the diamagnetism of the constituent atoms and the sample holder.

HF-EPR spectra of **1** were recorded at 4.5 K on polycrystalline samples (20–25 mg) by using a homodyne spectrometer associated with a 15/17-T superconducting magnet and a frequency range from 52 to 610 GHz. Detection was provided with an InSb hot electron bolometer (QMC Ltd., Cardiff, UK). The magnetic field was modulated at 50 kHz for detection purposes. A Stanford Research Systems SR830 lock-in amplifier converted the modulated signal to dc voltage. The single-frequency spectra were simulated with the SPIN software.

Mössbauer spectra were recorded between 5 and 160 K on a strong-field Mössbauer spectrometer equipped with an Oxford Instruments Spectromag 4000 cryostat containing an 8 T split-pair superconducting magnet. The spectrometer was operated in a constant acceleration mode in transmission geometry. The isomer shifts were referenced against that of a room-temperature metallic iron foil. Analysis of the data was performed with a homemade program^[73,74] that was adapted to treat the quantum spin admixture.

FD-FT THz-EPR data were acquired at the THz-EPR user station of the electron storage ring BESSY II. The setup is described in detail elsewhere.^[46,75] THz coherent synchrotron radiation (CSR) or broadband, unpolarized THz radiation emitted by the Hg arc lamp of a Fourier transform infrared (FTIR) spectrometer (Bruker IFS 125) were used as broad band (~ 4–50 cm⁻¹ and >12 cm⁻¹, respectively) excitation sources. The radiation was transmitted by a quasi-optical evacuated transmission line through the FTIR spectrometer and focused on the sample contained in a 10 T superconducting magnet (Oxford Spectromag). Spectra were recorded in Voigt geometry. The transmitted signal was detected by a Si bolometer detector (IR labs) and Fourier-transformed to yield frequency-domain EPR spectra. The experimental resolution was 0.5 cm⁻¹. Polycrystalline **1** (23 mg) was homogenized in a mortar with polyethylene (PE) powder (36 mg) and pressed into a pellet mounted in the variable-temperature insert of the magnet. FD-FT THz-EPR, as an FTIR-based technology, requires the measurement of a reference spectrum. Referencing between spectra recorded at different temperatures or fields was done as described elsewhere.^[46,62]

Frequency-domain spectra were simulated using the *EasySpin* toolbox,^[76–78] The spin Hamiltonian included the electron-Zeeman and the ZFS interactions:

$$\hat{H}_{\text{Spin}} = \underbrace{\mu_B \mathbf{B}_0 \mathbf{g} \hat{S}}_{\hat{H}_{\text{Zeeman}}} + D \left(\hat{S}_z^2 - \frac{1}{3} S(S+1) \right) + \underbrace{E (\hat{S}_x^2 - \hat{S}_y^2)}_{\hat{H}_{\text{ZFS}}} \quad (5)$$

where μ_B is the Bohr magneton, \mathbf{B}_0 the external magnetic field, \mathbf{g} the g matrix, \hat{S} the electron spin operator. The \mathbf{g} and \mathbf{D} (ZFS) interaction matrices were assumed to be collinear. The relative transmittance T in MDS at two magnetic fields B_i and B_j , experimentally obtained from the measured spectral intensities $I \text{Exp} = I_{B_j}/I_{B_i}$ as, are calculated from the simulated absorbance spectra A as $T_{\text{sim}} = 10^{A_{B_j} - A_{B_i}}$.

High-field THz spectra (FIRMS) were collected at the National High Magnetic Field Laboratory using a Bruker Vertex 80v FT-IR spectrometer coupled with a 17 T vertical-bore superconducting magnet in Voigt configuration. The experimental setup was equipped with a mercury lamp and a composite silicon bolometer (Infrared Laboratories), as a THz radiation source and detector, respectively. An *n*-eicosane pellet containing the studied compound (~ 7 mg) was measured in the spectral region between 14 and 730 cm⁻¹ (0.42–22 THz) with a resolution of 0.3 cm⁻¹ (9 GHz). Both sample and bolometer were cooled by a low-pressure helium gas to the temperature of 4.6 K. The relative transmittance spectra were calculated as the THz intensity spectrum at each magnetic field divided by the THz intensity spectrum averaged for all fields.

Single crystal X-ray diffraction: X-ray diffraction data of **1** was collected on a Bruker-Nonius X8APEXII CCD area detector diffractometer using graphite-monochromated Mo-K α radiation at T = 90 K. All calculations for data reduction, structure solution, and refinement were done through the SAINT^[52] and SADABS^[79,80] programs. The structure was solved with the SHELXS structure solution program, using the Patterson method. The model was refined with version 2013/4 of SHELXL against F² on all data by full-matrix least squares.^[81–83] All non-hydrogen atoms were refined with anisotropic displacement parameters. All the hydrogen atoms of the ligand were set in calculated position and refined isotropically using the riding model. Hydrogen atoms on the coordinated water molecules were found and refined with restraints on bond distance and angles. Chlorine and oxygen atoms of the perchlorate anions have been found to be statistically disordered (for symmetry) on two positions. Accordingly atom O(5) has been refined with a 0.5 of occupancy factor. The final geometrical calculations and the graphical manipulations were carried out with the PLATON package^[84,85] and CRYSTAL MAKER.^[86] Crystallographic data for compound **1** is given in Table S1. Crystallographic data for the structure reported in this paper has been deposited with the Cambridge

Crystallographic Data Centre as supplementary publication CCDC 1872265. The comments for the main alerts A and B are described in the CIF using the validation report form (vrf).

Computational details: The parameters that determine the axial (D) and rhombic (E) components of the local zero-field splitting (ZFS) of **1** were estimated from theoretical calculations based on density functional theory (DFT). Calculations were carried out on the experimental geometry with version 4.0 of the ORCA programme^[87] using the PBE and BP functionals,^[88–91] the resolution of the identity (RI) approximation,^[92,93] and the auxiliary TZV/J Coulomb fitting basis sets.^[94–98] All calculations were done in solution, including electronic effects of the solvent (acetonitrile) by “conductor-like polarizable continuum model”^[99] where the cavity that accommodates the molecule is built using the GEPOL algorithm.^[100–102] The spin-orbit and spin-spin coupling operators were based on the SOMF scheme.^[103,104] Coupled perturbed (CP) and Pederson-Khanna (PK) methods were used in the calculation of the spin-orbit contribution to the ZFS.^[105,106]

DFT calculations were carried out through the Gaussian 09 package in order to estimate the magnitude of the intermolecular magnetic couplings.^[107] These calculations were performed with the CAM-B3LYP hybrid functional,^[90,108–110] the quadratic convergence approach and a guess function generated with the fragment tool of the same program. Triple- ζ all electron basis set proposed by Ahlrichs et al. adding an extra p polarization function were employed for all atoms.^[95] The study was done using models including two neighbouring iron(III) complexes in their experimental geometries. The magnetic coupling states were obtained from the relative energies of the broken-symmetry (BS) singlet spin state from the high-spin state with parallel local spin moments. Details about the use of the broken-symmetry approach to evaluate magnetic coupling constants can be found in the literature.^[111–113] A polarizable continuum model (PCM) was introduced in the calculations with the parameters corresponding to acetonitrile.^[114] The optimization of molecular geometry on a mononuclear iron(III) complex was done starting from the experimental geometry of **1** and using the PBE functional as implemented in Gaussian09 packages.^[88,91] To improve the goodness of the calculated analytical vibrational frequencies, the restricted conditions were imposed in the self-consistent convergence of the wave-function and in the evaluation of the bi-electronic integrals (very tight and ultrafine, respectively) for the geometry optimization and evaluation of the vibrational modes. The calculated values of the D and ED parameters shown in Table S5 were made on the last optimized geometry with the PBE functional.

Acknowledgements

This work was financially supported by the MCCC (PID2019-109735GB-I00 and CTQ2016-75068-P), the Generalitat Valenciana (Project PROMETEOII/2014/070), “María de Maeztu” Excellence Unit by Mineco (MDM-2014-0538) and the Ministero dell’Istruzione, dell’Università e della Ricerca (Italy). M. V-C. acknowledges MINECO for a Juan de la Cierva research fellowship. G.B. and M.C. thank the Labex ARCANE (grant ANR-11-LABX-0003-01) and the Labex CBH-EUR-GS (grant ANR-17-EURE-0003) for financial support. Thanks are also extended to the “Fondo per il finanziamento delle attività base di ricerca” (D.A.). HFEP and FIRMS studies were supported by the NHMFL, which is funded by the NSF through a Cooperative Agreement DMR 1644779 and the State of Florida. We thank Dr. A. Ozarowski for

his EPR simulation and fit software SPIN. The authors are grateful to Dr. Karsten Holldack and Dirk Ponwitz for experimental assistance with the FD-FT THz-EPR experiments. Support of the FD-FT THz-EPR experiments through HZB's user program and DFG SPP 1601 are gratefully acknowledged.

Keywords: Single-ion magnet • anisotropy • iron • porphyrinoids • spin admixture

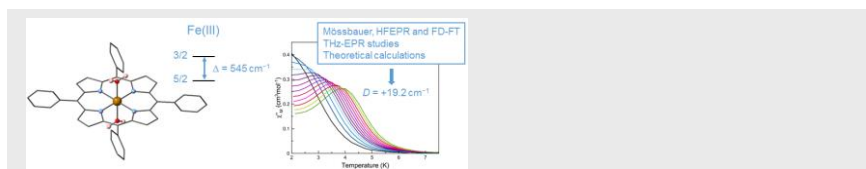
- [1] D. Gatteschi, R. Sessoli, J. Villain, *Molecular Nanomagnets*, Oxford University Press, **2006**.
- [2] M. D. Jenkins, D. Zueco, O. Roubeau, G. Aromí, J. Majer, F. Luis, *Dalton Trans.* **2016**, *45*, 16682–16693.
- [3] A. Gaita-Ariño, F. Luis, S. Hill, E. Coronado, *Nat. Chem.* **2019**, *11*, 301–309.
- [4] C.-J. Yu, M. J. Graham, J. M. Zadrozny, J. Niklas, M. D. Krzyaniak, M. R. Wasielewski, O. G. Poluektov, D. E. Freedman, *J. Am. Chem. Soc.* **2016**, *138*, 14678–14685.
- [5] K. Bader, D. Dengler, S. Lenz, B. Endeward, S.-D. Jiang, P. Neugebauer, J. van Slageren, *Nat. Commun.* **2014**, *5*, 5304.
- [6] A. Urtizberea, E. Natividad, P. J. Alonso, M. A. Andrés, I. Gascón, M. Goldmann, O. Roubeau, *Adv. Funct. Mater.* **2018**, *28*, 1801695.
- [7] M. Atzori, E. Morra, L. Tesi, A. Albino, M. Chiesa, L. Sorace, R. Sessoli, *J. Am. Chem. Soc.* **2016**, *138*, 11234–11244.
- [8] M. Feng, M. L. Tong, *Chem. Eur. J.* **2018**, *24*, 7574–7594.
- [9] G. A. Craig, M. Murrie, *Chem. Soc. Rev.* **2015**, *44*, 2135–2147.
- [10] S. Gómez-Coca, D. Aravena, R. Morales, E. Ruiz, *Coord. Chem. Rev.* **2015**, *289–290*, 379–392.
- [11] J. M. Frost, K. L. M. Harriman, M. Murugesu, *Chem. Sci.* **2016**, *2470–2491*.
- [12] R. Herchel, L. Váhovská, I. Potočňák, Z. Trávníček, *Inorg. Chem.* **2014**, *53*, 5896–8.
- [13] E. Colacio, J. Ruiz, E. Ruiz, E. Cremades, J. Krzystek, S. Carretta, J. Cano, T. Guidi, W. Wernsdorfer, E. K. Brechin, *Angew. Chemie Int. Ed.* **2013**, *52*, 9130–9134.
- [14] W. Huang, T. Liu, D. Wu, J. Cheng, Z. W. Ouyang, C. Duan, *Dalton Trans.* **2013**, *42*, 15326.
- [15] J. M. Zadrozny, J. Liu, N. A. Piro, C. J. Chang, S. Hill, J. R. Long, *Chem. Commun.* **2012**, *48*, 3927–3929.
- [16] D. Wu, X. Zhang, P. Huang, W. Huang, M. Ruan, Z. W. Ouyang, *Inorg. Chem.* **2013**, *52*, 10976–10982.
- [17] S. Gómez-Coca, A. Urtizberea, E. Cremades, P. J. Alonso, A. Camón, E. Ruiz, F. Luis, *Nat. Commun.* **2014**, *5*, 4300–4307.
- [18] J. Vallejo, I. Castro, R. Ruiz-García, J. Cano, M. Julve, F. Lloret, G. De Munno, W. Wernsdorfer, E. Pardo, *J. Am. Chem. Soc.* **2012**, *134*, 15704–15707.
- [19] S. Hino, M. Maeda, K. Yamashita, Y. Kataoka, M. Nakano, T. Yamamura, H. Nojiri, M. Kofu, O. Yamamuro, T. Kajiwara, *Dalton Trans.* **2013**, *42*, 2683–2686.
- [20] Q. W. Li, R. C. Wan, Y. C. Chen, J. L. Liu, L. F. Wang, J. H. Jia, N. F. Chilton, M. L. Tong, *Chem. Commun.* **2016**, *52*, 13365–13368.
- [21] J. J. Le Roy, I. Korobkov, J. E. Kim, E. J. Schelter, M. Murugesu, *Dalton Trans.* **2014**, *43*, 2737–2740.
- [22] R. Boča, C. Rajnák, J. Titiš, D. Valigura, *Inorg. Chem.* **2017**, *56*, 1478–1482.
- [23] L. Escalera-Moreno, N. Suaud, A. Gaita-Ariño, E. Coronado, *J. Phys. Chem. Lett.* **2017**, *8*, 1695–1700.
- [24] M. Atzori, L. Tesi, S. Benci, A. Lunghi, R. Righini, A. Taschin, R. Torre, L. Sorace, R. Sessoli, *J. Am. Chem. Soc.* **2017**, *139*, 4338–4341.
- [25] A. Lunghi, F. Totti, R. Sessoli, S. Sanvito, *Nat. Commun.* **2017**, *8*, 14620–14626.
- [26] A. Lunghi, F. Totti, S. Sanvito, R. Sessoli, *Chem. Sci.* **2017**, *8*, 6051–6059.
- [27] C. A. P. Goodwin, D. Reta, F. Ortu, N. F. Chilton, D. P. Mills, *J. Am. Chem. Soc.* **2017**, *139*, 18714–18724.
- [28] F. Neese, E. I. Solomon, *Inorg. Chem.* **1998**, *37*, 6568–6582.
- [29] L. Wang, M. Zlatar, F. Vlahović, S. Demeshko, C. Philouze, F. Molton, M. Gennari, F. Meyer, C. Duboc, M. Gruden, *Chem. - A Eur. J.* **2018**, *24*, 5091–5094.
- [30] X. Feng, S.-J. Hwang, J.-L. Liu, Y.-C. Chen, M.-L. Tong, D. G. Nocera, *J. Am. Chem. Soc.* **2017**, *139*, 16474–16477.
- [31] S. Mossin, B. L. Tran, D. Adhikari, M. Pink, F. W. Heinemann, J. Sutter, R. K. Szilagyí, K. Meyer, D. J. Mindiola, *J. Am. Chem. Soc.* **2012**, *134*, 13651–13661.
- [32] J. Vallejo, A. Pascual-Álvarez, J. Cano, I. Castro, M. Julve, F. Lloret, J. Krzystek, G. De Munno, D. Armentano, W. Wernsdorfer, R. Ruiz-García, E. Pardo, *Angew. Chemie Int. Ed.* **2013**, *52*, 14075–14079.
- [33] Q. Ma, S. Zeng, X. Feng, W. Cao, H. Wang, J. Dou, J. Jiang, *Eur. J. Inorg. Chem.* **2016**, 4194–4198.
- [34] M. Nakamura, *Coord. Chem. Rev.* **2006**, *250*, 2271–2294.
- [35] W. R. Scheidt, C. A. Reed, *Chem. Rev.* **1981**, *81*, 543–555.
- [36] C. A. Reed, F. Guiset, *J. Am. Chem. Soc.* **1996**, *118*, 3281–3282.
- [37] M. M. Maltempo, *J. Chem. Phys.* **1974**, *61*, 2540–2547.
- [38] O. Kahn, *Molecular Magnetism*, Wiley-VCH, New York, **1993**.
- [39] W. R. Scheidt, I. A. Cohen, M. E. Kastner, *Biochemistry* **1979**, *18*, 3546–3552.
- [40] B. Cheng, W. R. Scheidt, *Acta Crystallogr. Sect. C Cryst. Struct. Commun.* **1995**, *51*, 1271–1275.
- [41] E. König, S. Kremer, *Ligand Field*, Springer US, Boston, MA, **1977**.
- [42] J. Vallejo, F. R. Fortea-Pérez, E. Pardo, S. Benmansour, I. Castro, J. Krzystek, D. Armentano, J. Cano, *Chem. Sci.* **2016**, *7*, 2286–2293.
- [43] J. Vallejo, E. Pardo, M. Viciano-Chumillas, I. Castro, P. Amoros, M. Deniz, C. Ruiz-Perez, C. Yuste-Vivas, J. Krzystek, M. Julve, F. Lloret, J. Cano, P. Amorós, M. Déniz, C. Ruiz-Pérez, C. Yuste-Vivas, J. Krzystek, M. Julve, F. Lloret, J. Cano, *Chem. Sci.* **2017**, *8*, 3694–3702.
- [44] A. Świttlicka, J. Palion-Gazda, B. Machura, J. Cano, F. Lloret, M. Julve, *Dalton Trans.* **2019**, *48*, 1404–1417.
- [45] J. Cano, VPMAG, University Of Valencia, Valencia, Spain, **2003**.
- [46] J. Nehrkor, K. Holldack, R. Bittl, A. Schnegg, *J. Magn. Reson.* **2017**, *280*, 10–19.
- [47] J. Krzystek, J. Telser, *Dalton Trans.* **2016**, *45*, 16751–16763.
- [48] J. Krzystek, S. A. Zvyagin, A. Ozarowski, S. Trofimenko, J. Telser, *J. Magn. Reson.* **2006**, *178*, 174–183.
- [49] A. Gismelseed, E. L. Bominaar, E. Bill, A. X. Trautwein, H. Winkler, H. Nasri, P. Doppelt, D. Mandon, J. Fischer, R. Weiss, *Inorg. Chem.*

- 1990, 29, 2741–2749.
- [50] M. M. Maltempo, T. H. Moss, K. Spartaian, *J. Chem. Phys.* **1980**, 73, 2100–2106.
- [51] T. Okamoto, E. Ohmichi, S. Okubo, H. Ohta, *J. Phys. Soc. Japan* **2018**, 87, 013702–013705.
- [52] SAINT, Computer Program, Bruker Analytical X-Ray Systems, Madison, WI, **2003**.
- [53] Y. Ping, D. Rocca, G. Galli, *Chem. Soc. Rev.* **2013**, 42, 2437–2469.
- [54] D. Escudero, *Acc. Chem. Res.* **2016**, 49, 1816–1824.
- [55] J. M. Herbert, X. Zhang, A. F. Morrison, J. Liu, *Acc. Chem. Res.* **2016**, 49, 931–941.
- [56] J. M. Carbonell, J. Cano, *DynVPMag*, Universitat De Valencia, Valencia, Spain, **2019**.
- [57] E. Lucaccini, L. Sorace, M. Perfetti, J.-P. Costes, R. Sessoli, *Chem. Commun.* **2014**, 50, 1648–1651.
- [58] N. Ge, Y.-Q. Zhai, Y.-F. Deng, Y.-S. Ding, T. Wu, Z.-X. Wang, Z. Ouyang, H. Nojiri, Y.-Z. Zheng, *Inorg. Chem. Front.* **2018**, 5, 2486–2492.
- [59] T. Minato, D. Aravena, E. Ruiz, K. Yamaguchi, N. Mizuno, K. Suzuki, *Inorg. Chem.* **2018**, 57, 6957–6964.
- [60] R. Sato, K. Suzuki, T. Minato, M. Shinoue, K. Yamaguchi, N. Mizuno, *Chem. Commun.* **2015**, 51, 4081–4084.
- [61] D. V. Behere, R. Birdy, S. Mitra, *Inorg. Chem.* **1981**, 20, 2786–2789.
- [62] J. Nehr Korn, B. M. Martins, K. Holldack, S. Stoll, H. Dobbek, R. Bittl, A. Schnegg, *Mol. Phys.* **2013**, 111, 2696–2707.
- [63] S. E. Stavretis, M. Atanasov, A. A. Podlesnyak, S. C. Hunter, F. Neese, Z. L. Xue, *Inorg. Chem.* **2015**, 54, 9790–9801.
- [64] D. R. Evans, C. A. Reed, *J. Am. Chem. Soc.* **2000**, 122, 4660–4667.
- [65] R. Ishikawa, R. Miyamoto, H. Nojiri, B. K. Breedlove, M. Yamashita, *Inorg. Chem.* **2013**, 52, 8300–8302.
- [66] A. Grigoropoulos, M. Pissas, P. Papatolis, V. Psycharis, P. Kyritsis, Y. Sanakis, *Inorg. Chem.* **2013**, 52, 12869–12871.
- [67] D. H. Moseley, S. E. Stavretis, K. Thirunavukkuarasu, M. Ozerov, Y. Cheng, L. L. Daemen, J. Ludwig, Z. Lu, D. Smirnov, C. M. Brown, A. Pandey, A. J. Ramirez-Cuesta, A. C. Lamb, M. Atanasov, E. Bill, F. Neese, Z.-L. Xue, *Nat. Commun.* **2018**, 9, 2572–2582.
- [68] L. Escalera-Moreno, J. J. Baldoví, A. Gaita-Ariño, E. Coronado, *Chem. Sci.* **2018**, 9, 3265–3275.
- [69] L. Escalera-Moreno, N. Suaud, A. Gaita-Ariño, E. Coronado, *J. Phys. Chem. Lett.* **2017**, 8, 1695–1700.
- [70] M. Atzori, L. Tesi, E. Morra, M. Chiesa, L. Sorace, R. Sessoli, *J. Am. Chem. Soc.* **2016**, 138, 2154–2157.
- [71] K. Bader, M. Winkler, J. van Slageren, *Chem. Commun.* **2016**, 52, 3623–3626.
- [72] A. D. Adler, F. R. Longo, F. Kampas, J. Kim, *J. Inorg. Nucl. Chem.* **1970**, 32, 2443–2445.
- [73] C. Charavay, S. Segard, F. Edon, M. Clémancey, G. Blondin, *SimuMoss Software*, Univ. Grenoble Alpes, CEA/BIG, CNRS, Grenoble, **2012**.
- [74] M. Carboni, M. Clémancey, F. Molton, J. Pécaut, C. Lebrun, L. Dubois, G. Blondin, J. M. Latour, *Inorg. Chem.* **2012**, 51, 10447–10460.
- [75] K. Holldack, A. Schnegg, *J. Large-scale Res. Facil. JLSRF* **2016**, 2, A51.
- [76] J. Nehr Korn, J. Telser, K. Holldack, S. Stoll, A. Schnegg, *J. Phys. Chem. B* **2015**, 119, 13816–13824.
- [77] J. Nehr Korn, A. Schnegg, K. Holldack, S. Stoll, *Phys. Rev. Lett.* **2015**, 114, 010801.
- [78] S. Stoll, A. Schweiger, *J. Magn. Reson.* **2006**, 178, 42–55.
- [79] L. Krause, R. Herbst-Irmer, G. M. Sheldrick, D. Stalke, *J. Appl. Crystallogr.* **2015**, 48, 3–10.
- [80] G. M. SADABS, Program for Absorption Correction Sheldrick, **2003**.
- [81] G. M. Sheldrick, *Acta Crystallogr. Sect. C Struct. Chem.* **2015**, 71, 3–8.
- [82] G. M. Sheldrick, *Acta Crystallogr. A* **2008**, 64, 112–122.
- [83] SHELXTL-2013/4, **2013**.
- [84] A. L. Spek, *Acta Crystallogr. Sect. C Struct. Chem.* **2015**, 71, 9–18.
- [85] A. L. Spek, *Acta Crystallogr. Sect. D Biol. Crystallogr.* **2009**, 65, 148–155.
- [86] D. Palmer, **1996**.
- [87] F. Neese, *Wires Comput Mol Sci* **2012**, 2, 73–78.
- [88] J. P. Perdew, K. Burke, M. Ernzerhof, *Phys. Rev. Lett.* **1997**, 78, 1396–1396.
- [89] J. P. Perdew, K. Burke, M. Ernzerhof, *Phys. Rev. Lett.* **1996**, 77, 3865–3868.
- [90] A. D. Becke, *Phys. Rev. A* **1988**, 38, 3098–3100.
- [91] J. P. Perdew, *Phys. Rev. B* **1986**, 33, 8822–8824.
- [92] F. Neese, *J. Comput. Chem.* **2003**, 24, 1740–1747.
- [93] D. Ganyushin, N. Gilka, P. R. Taylor, C. M. Marian, F. Neese, *J. Chem. Phys.* **2010**, 132, 144111.
- [94] A. Schäfer, H. Horn, R. Ahlrichs, *J. Chem. Phys.* **1992**, 97, 2571.
- [95] A. Schäfer, C. Huber, R. Ahlrichs, A. Schafer, C. Huber, R. Ahlrichs, *J. Chem. Phys.* **1994**, 100, 5829–5835.
- [96] K. Eichkorn, O. Treutler, H. Öhm, M. Häser, R. Ahlrichs, *Chem. Phys. Lett.* **1995**, 240, 283–289.
- [97] K. Eichkorn, O. Treutler, H. Öhm, M. Häser, R. Ahlrichs, *Chem. Phys. Lett.* **1995**, 242, 652–660.
- [98] K. Eichkorn, F. Weigend, O. Treutler, R. Ahlrichs, *Theor. Chem. Acc* **1997**, 97, 119–124.
- [99] V. Barone, M. Cossi, *J. Phys. Chem. A* **1998**, 102, 1995–2001.
- [100] J. L. Pascual-Ahuir, E. Silla, *J. Comput. Chem.* **1990**, 11, 1047–1060.
- [101] E. Silla, I. Tuñón, J. L. Pascual-Ahuir, *J. Comput. Chem.* **1991**, 12, 1077–1088.
- [102] J. L. Pascual-Ahuir, E. Silla, I. Tuñón, *J. Comput. Chem.* **1994**, 15, 1127–1138.
- [103] B. A. Heß, C. M. Marian, U. Wahlgren, O. Gropen, *Chem. Phys. Lett.* **1996**, 251, 365–371.
- [104] F. Neese, *J. Am. Chem. Soc.* **2006**, 128, 10213–10222.
- [105] F. Neese, *J. Chem. Phys.* **2007**, 127, 164112.
- [106] M. R. Pederson, S. N. Khanna, *Phys. Rev. B - Condens. Matter Mater. Phys.* **1999**, 60, 9566–9572.
- [107] Gaussian-09, M. J. Frisch, G. W. Trucks, H. B. Schlegel, G. E. Scuseria, M. A. Robb, J. R. Cheeseman, G. Scalmani, V. Barone, B. Mennucci, G. A. Petersson, H. Nakatsuji, M. Caricato, X. Li, H. P. Hratchian, A. F. Izmaylov, J. Bloino, G. Zheng, J. L. Sonnenberg, M. Hada, M. Ehara, K. Toyota, R. Fukuda, J. Hasegawa, M. Ishida, T. Nakajima, Y. Honda, O. Kitao, H. Nakai, T. Vreven, J. A.

- Montgomery, J. E. Peralta, F. Ogliaro, M. Bearpark, J. J. Heyd, E. Brothers, K. N. Kudin, V. N. Staroverov, R. Kobayashi, J. Normand, K. Raghavachari, A. Rendell, J. C. Burant, S. S. Iyengar, J. Tomasi, M. Cossi, N. Rega, J. M. Millam, M. Klene, J. E. Knox, J. B. Cross, V. Bakken, C. Adamo, J. Jaramillo, R. Gomperts, R. E. Stratmann., O. Yazyev, A. J. Austin, R. Cammi, C. Pomelli, J. W. Ochterski, R. L. Martin, K. Morokuma, V. G. Zakrzewski, G. A. Voth, P. Salvador, J. J. Dannenberg, S. Dapprich, A. D. Daniels, Ö. Farkas, J. B. Foresman, J. V. Ortiz, D. J. Cioslowski, D. J. Fox, **2009**.
- [108] C. Lee, W. Yang, R. G. Parr, *Phys. Rev. B* **1988**, 37, 785–789.
- [109] A. D. Becke, *J. Chem. Phys.* **1993**, 98, 5648–5652.
- [110] T. Yanai, D. P. Tew, N. C. Handy, *Chem. Phys. Lett.* **2004**, 393, 51–57.
- [111] E. Ruiz, A. Rodríguez-Forteza, J. Cano, S. Alvarez, P. Alemany, *J. Comput. Chem.* **2003**, 24, 982–989.
- [112] E. Ruiz, J. Cano, S. Alvarez, P. Alemany, *J. Comput. Chem.* **1999**, 20, 1391–1400.
- [113] E. Ruiz, J. Cano, S. Alvarez, P. Alemany, *J. Am. Chem. Soc.* **1998**, 120, 11122–11129.
- [114] J. Tomasi, B. Mennucci, E. Cancès, *J. Mol. Struct. Theochem* **1999**, 464, 211–226.

Entry for the Table of Contents

FULL PAPER



Marta Viciano-Chumillas,^[a] Geneviève Blondin,^[b] * Martin Clémancey,^[b] J. Krzystek,^[c] * Mykhaylo Ozerov,^[c] Donatella Armentano,^[d] Alexander Schnegg,^[e] Thomas Lohmiller,^[f] Joshua Telser,^[g] Francesc Lloret,^[a] and Joan Cano^[a] *

Unusually large zero-field splitting and single-ion magnet behaviour in an iron(III) porphyrin complex.

Page No. – Page No.

Single-Ion Magnetic Behaviour in an Iron(III) Porphyrin Complex: A Dichotomy between High-Spin and 5/2-3/2 Spin Admixture